



Physical design and multi-particle simulations of a compact IH-DTL with KONUS beam dynamics for proton therapy

Jian Qiao^{1,2} · Xiu-Cui Xie¹ · De-Ming Li^{1,3} · Yue-Hu Pu^{1,3}

Received: 10 December 2019 / Revised: 21 April 2020 / Accepted: 22 April 2020 / Published online: 17 June 2020

© China Science Publishing & Media Ltd. (Science Press), Shanghai Institute of Applied Physics, the Chinese Academy of Sciences, Chinese Nuclear Society and Springer Nature Singapore Pte Ltd. 2020

Abstract A compact room-temperature inter-digital H-mode (IH) drift tube linac (DTL) with Kombinierte Null Grad Struktur beam dynamics is proposed in this paper. The proposed IH-DTL, which operates at 325 MHz, accelerates 18 mA proton particles from 3.0 to 7.0 MeV as part of a proton synchrotron-based therapy system. It is composed of two main sections, namely a bunching section (-30°) and accelerating section (0°). There is no transverse focusing element inside the cavity, which increases the acceleration gradient and reduces the cavity length and power consumption. In our physical designs, LORASR code is utilized for beam dynamics design and multi-particle simulations. The synchronous particle energy, injection phase, and acceleration voltage of each gap are optimized carefully to increase transmission efficiency while minimizing beam emittance growth and beam loss. The total length of the cavity is 0.82 m and the acceleration gradient reaches 4.88 MV/m, resulting in a transmission efficiency of 100% and beam emittance growth less than 10%. The details of the specific work undertaken in this study are presented in this paper.

Keywords Proton therapy · Linac injector · KONUS beam dynamics · IH-DTL

1 Introduction

Radiation therapy using protons and heavy ions is increasing in popularity based on its distinct physical characteristics in terms of energy deposition, excellent therapeutic effects, and fewer side effects in many specific tumor treatments compared to conventional photon radiotherapy [1]. It has significant advantages for killing cancer cells. The Shanghai Institute of Applied Physics has been devoted to basic research on proton therapy for the past 10 years [2–4]. The Advanced Proton Therapy Facility (APTR), which is illustrated in Fig. 1, was developed as the first full-service proton radiotherapy facility [5]. Figure 1a presents a scheme of the injector system, which was purchased abroad, in operation. This system mainly consists of a dual-plasma pulse source, low-energy beam transport line, radio-frequency quadrupole (RFQ), and Alvarez drift tube linac (DTL). The RFQ and the Alvarez DTL in the original scheme are connected directly with no matching elements between them. As a key technique of the APTR complex, an upgrade for this injector system has been proposed to accelerate the processes of location and industrialization. Figure 1b presents this recent upgrade scheme.

In this paper, the physical design and multi-particle simulations of the post-accelerator (DTL) based on LORASR code are introduced. The specific design indicators for the proposed DTL are listed in Table 1.

This work was supported by the Ministry of Science and Technology of the People's Republic of China under the National Key Research and Development Program (No. 2016YFC0105408).

✉ Yue-Hu Pu
puyuehu@sinap.ac.cn

¹ Shanghai Institute of Applied Physics, Chinese Academy of Sciences, Shanghai 201800, China

² University of the Chinese Academy of Sciences, Beijing 100049, China

³ Shanghai APACRON Particle Equipment Company Ltd., Shanghai 210800, China

Fig. 1 (Color online) Overall layout of the APTR complex, as well as original and upgraded schemes for the injector

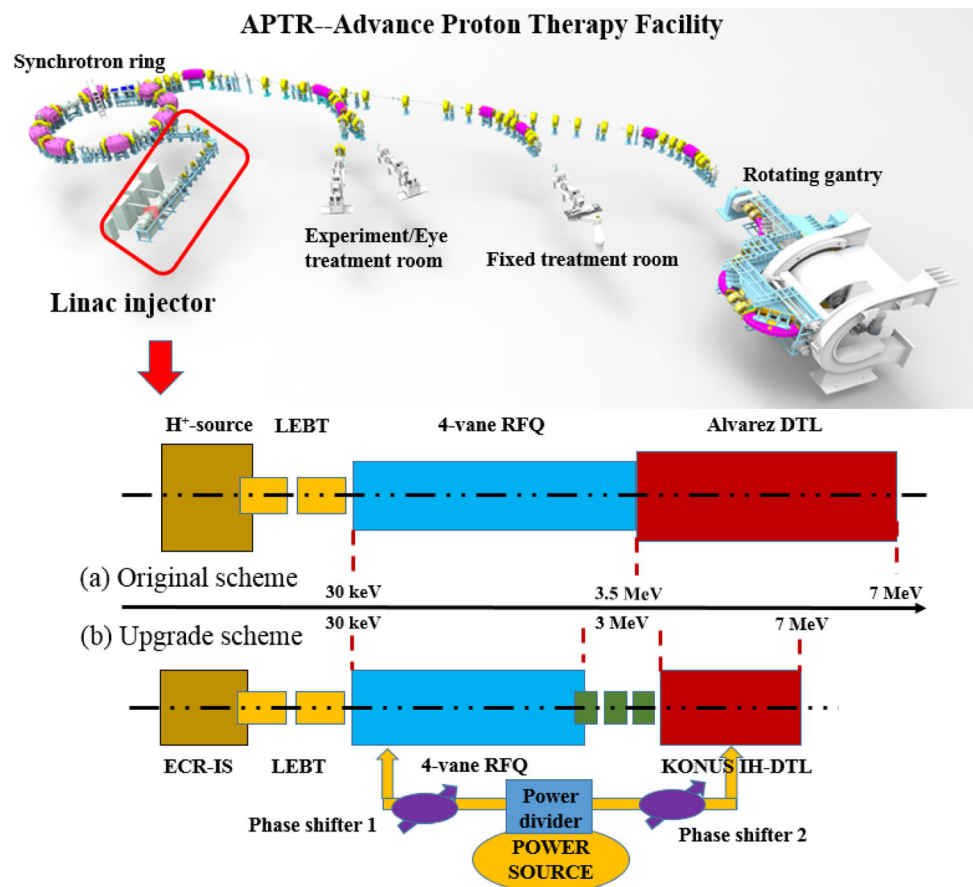


Table 1 Design indicators for the proposed DTL

Parameters	Values
Frequency (MHz)	325
Particle type	H ⁺
Input/output energy (MeV)	3/7
Peak current (mA)	18
Maximum duty factor	0.1%
Transmission efficiency	≥ 95%
Output energy spread	≤ 1.5%
Output phase width (deg)	≤ ± 30
Output transverse norm. Root mean squared (RMS) emittance (π mm mrad)	≤ 0.24

2 Design strategy

2.1 Selection of design principles and cavity type

For a low-energy, high-current hadron linac, the non-linear defocusing effect is an unavoidable issue. Typically, to achieve transverse focusing, longitudinal bunching, and acceleration, three main types of DTL beam dynamics principles are implemented in the low-energy range, namely negative synchronous phase structure (NSPS) [6], alternative phase focusing (APF) [7–9], and combined

zero-degree structure (KONUS) [6, 10] DTL beam dynamics. The Alvarez DTL, which uses the NSPS dynamics principle, has been adopted for many proton injectors, including the Heavy Ion Medical Accelerator in Chiba (HIMAC) [11]. Inter-digital H-mode (IH)-DTLs with APF and KONUS beam dynamics are also used in various proton and heavy-ion radiation therapy facilities, including the upgraded HIMAC* facility in Japan [7, 9], Heidelberg Ion-Beam Therapy Center (HIT) in Europe [12], and Centro Nazionale di Adroterapia Oncologica (CNAO) in Italy [13]. Different design strategies are

adopted in various facilities. Table 2 lists the relevant parameters of DTLs for several representative proton and heavy-ion radiation therapy facilities in operation around the world.

The main differences between the three types of dynamics mentioned above are listed in Table 3 [20].

In the NSPS dynamics principle, which is applied in the Alvarez DTL structure, quadrupole magnets are set inside the drift tube, which causes an increase in the drift tube volume, capacitance in the cavity load, and power loss. Furthermore, the electromagnetic field mode (TM_{010}) leads to a decrease in shunt impedance, thereby reducing acceleration gradients. The maximum acceleration gradient is approximately 3.5 MV/m. The negative acceleration phase, which is generally -30° , also limits the growth of effective acceleration gradients.

The main advantages of this conventional structure can be summarized as follows:

- (a) Transverse focusing magnets inside the drift tube ensure easy transverse matching.
- (b) A negative phase is used to accept and accelerate particles, ensuring enhanced acceptance, fewer nonlinear effects during acceleration, and easy longitudinal bunching.
- (c) Small longitudinal and transversal emittance growth under consistent error conditions.

In contrast, the main disadvantages can be summarized as follows:

- (1) Greater transverse dimension of the cavity.
- (2) Low RF efficiency and high thermal loss.
- (3) Difficulties in the processing and installation of drift tubes with magnets, particularly in terms of ensuring that the magnetic center coincides with the center of the beam hole.

In APF DTL dynamics, focusing and defocusing strengths are enhanced by selecting alternating positive and negative synchronous phases for the RF acceleration field at each gap to achieve particle stability during transverse

and longitudinal movements. The absence of focusing magnets in the cavity is the most attractive feature of APF because it can significantly reduce production costs [18]. However, this method depends heavily on the arrangement of synchronous phases to achieve transverse focusing and longitudinal bunching. The length of the drift tube is not gradually lengthened, but changes nonlinearly, which leads to a decrease in the dynamic aperture and reduced acceptance. Transverse emittance growth is relatively large based on the fact that transverse particle oscillations are strongly affected by longitudinal motion in the low-energy range. Additionally, beam motion is sensitive to errors and the accuracy requirements of machining and assembly are extremely strict [20, 21].

The main feature of KONUS dynamics is the separation of longitudinal bunching, acceleration, and transverse focusing to maintain the stability of particle motion and acceleration gradients. Transverse motion is maintained within a reasonable range by using magnets, and longitudinal motion is ensured by several negative phase gaps. Slim drift tubes result in a low capacity load per unit length and increased power efficiency. Additionally, emittance growth is smaller, acceptance is larger, transmission efficiency and beam current are increased, and the quality of output beams is enhanced compared to APF under the same conditions [20, 21].

Furthermore, an IH-type structure [20–26] is adopted to increase acceleration gradients while reducing power consumption and cavity length. Based on integrated processing technology, the machining and installation process is also relatively simple.

Considering the pros and cons of these three principles in terms of various factors, including cost, power consumption, acceleration efficiency, cavity length, and project risk, the KONUS beam dynamics principle combined with an IH-type RF structure was selected as the final choice for the upgraded injector.

Table 2 Parameter summary for proton and heavy-ion linac injectors in operation worldwide

Name	DTL energy range and type	q/m ratio	Frequency (MHz)
HIMAC [11]	0.8–6 MeV/u Alvarez DTL	$\geq 1/7$	100
HIMAC ^a [9, 14]	0.61 to 4–8 MeV/u APF IH-DTL	1/3 (C^{4+})	200.0
HIT [12, 15]	0.4–7 MeV/u KONUS IH-DTL	1/3 (H_3^+ and C^{4+})	216.8
CSNS [16]	3.0–80 MeV Alvarez DTL	1 (H^-)	324.0
CPHS [17]	3.0–13.0 MeV Alvarez DTL	1 (H^+)	325.0
HICAT [18]	0.4–7 MeV/u KONUS IH-DTL	1/3 (C^{4+})	216.8
CNAO [13]	0.4–7 MeV/u KONUS IH-DTL	1/3 (H_3^+ and C^{4+})	216.8
SNS [19]	2.5–86 MeV Alvarez DTL	1 (H^-)	402.5

^aUpgraded HIMAC facility (Japan)

Table 3 Comparison of three main-stream DTL beam dynamics principles

Principles	Alvarez	APF IH-DTL	KONUS IH-DTL
Applicable β range	0.05–0.4	0.01–0.2	0.01–0.25
The length of unit	$\beta\lambda$	$\beta\lambda/2$	$\beta\lambda/2$
Operation mode	TM ₀₁₀	TE ₁₁₀	TE ₁₁₀
Acceleration phase	Negative phase	Alter. phase	Zero/neg. phase
Effective shunt impedance (M Ω /m)	40–80	50–200	50–500
Applicable frequency range (MHz)	100–400	30–500	30–500

2.2 KONUS beam dynamics principle

Figure 2 presents a KONUS structure period, which typically consists of three components, namely a focusing lens (quadrupole doublets, triplets, or solenoids in the case of a superconducting linac), negative synchrotron phase section, and zero-degree section [6, 10, 20–25]. It is also defined by a half-triplet, followed by a re-bunching section and zero-degree section next to a second half-triplet [10]. Different definitions of the composition of a KONUS period are related to transverse phase advance. Transverse focusing is achieved by quadrupole triplets. Longitudinal bunching and acceleration are achieved by optimizing bunch center motion. Generally, re-bunching sections are placed in front of zero-degree sections to maintain the stability of longitudinal motion.

The synchrotron particle and bunch center are defined independently. The energy difference and phase width of the first acceleration gap can be optimized according to the following conditions [22–25].

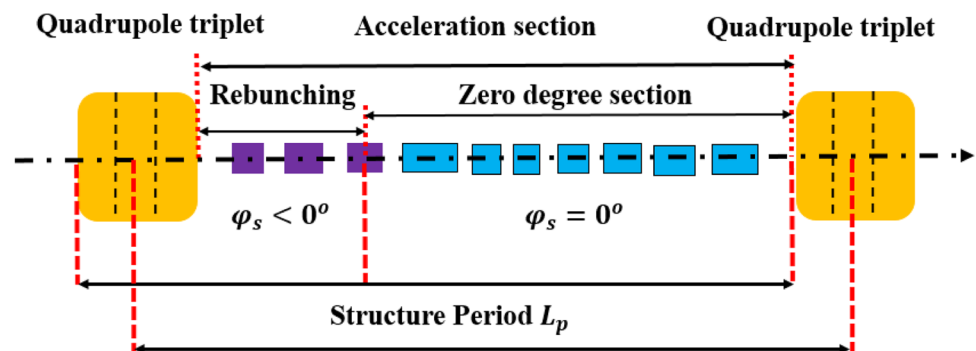
In the re-bunching section, the energy and phase of the centroid particle (index “c”) are identically equal to those of the synchronous particles (index “s”), meaning

$$\begin{cases} W_c = W_s \\ \varphi_c = \varphi_s \end{cases} \quad (1)$$

In contrast, in the zero-degree section, they should be

$$\begin{cases} \Delta W = (W_c - W_s) > 0 \\ \Delta\varphi = (\varphi_c - \varphi_s) = \varphi_c \end{cases} \quad (2)$$

Fig. 2 (Color online) Diagram of a KONUS structure period



When particles reach the first gap in the zero-degree section, the bunch center, which has a surplus of injection energy relative to the zero-degree synchronous particle (ZDSP), moves from the positive to the negative RF phase gradually. Once the energy of the beam centroid is close to that of the ZDSP, the zero-degree section ends and a triplet followed by a re-bunching section begins. Then, the phase and energy of the bunch center are redefined and the particles enter a new period.

In this design, to improve the acceleration gradient and reduce power loss, the cavity is only composed of a negative phase bunching section and zero-degree section. Additionally, the lenses are moved outside the cavity. These changes are also beneficial in terms of integrated processing, installation, and collimation because they combine the features of APF with the advantages of the KONUS principle, which is an excellent choice in terms of miniaturization of the injector and several specific application scenarios [26].

2.3 Design flow

Figure 3 illustrates the cavity design processes in detail. These processes can be roughly divided into the following three sections:

- (1) Beam dynamics design
- (2) Multi-particle simulation
- (3) RF design and simulation

The LORASR code [27], which was developed for KONUS beam dynamics design, has been verified and

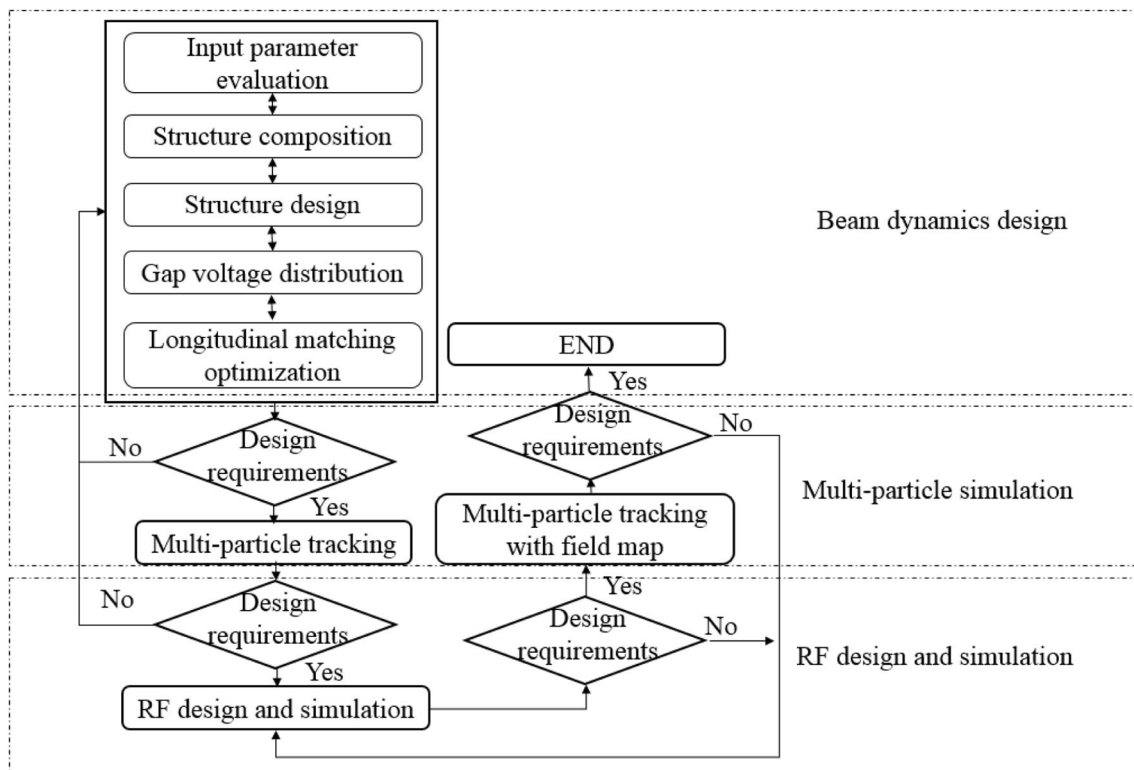


Fig. 3 Detailed cavity design processes

benchmarked by several linacs in operation, including the GSI-HLI, GSI-HSI, CERN Linac3, and TRIUMF ISAC-1. In this project, this code was adopted for beam dynamics design and multi-particle simulations. The cooperative iteration optimization of beam dynamics design and multi-particle simulations should be considered during the design process. The Computer Simulation Technology Microwave Studio [28] was utilized to perform RF calculations. The shunt impedance, surface peak electric field, power consumption, voltage distribution, and quality factor (Q_0 factor) were considered.

The three sections in the figure above are interconnected and reliant on each other. First, based on the design parameters, specific dynamics design is conducted for the inner structures, gap voltage, transverse focusing, and longitudinal matching. The RF model structure of the cavity is also determined. Second, multi-particle tracking with space-charge effect is simulated. In these two sections, parameter iterative optimization is performed using a nonlinear optimization algorithm. Third, RF structural design and simulations are conducted based on the design results of the previous sections. The RF characteristic parameters are evaluated, and the field distributions are utilized in multi-particle simulations for secondary inspection. In this paper, we mainly focus on physical design and multi-particle simulations with analytical fields.

Detailed dynamics designs and simulation processes are described below.

3 Dynamics designs and comparisons

3.1 Selection and optimization of design parameters

Several constraints and key parameters for the design of the 3–7 MeV IH-DTL that should be carefully considered are described below.

(1) Choice of RFQ-DTL transition energy

There is a tradeoff between the adequate maximum output energy of the RFQ and the minimum acceptable input energy for the IH-DTL. Covering a larger energy range for the RFQ reduces acceleration efficiency and leads to various issues related to tank length, field flatness, and coupling between structure cells. Furthermore, the minimum length of the drift tube, which is approximately 20 mm [6], is restricted by the limits of modern machining technology. By referring to the parameters of other facilities, the injection energy was set to 3 MeV.

(2) Geometric length of the transition cell

The transition cell can be adjusted by modulating the length of gaps or mounting a longer drift tube to ensure that

the phase shift slides from -35° or -30° to 0° . Generally, the length of the transition cell is defined as

$$L_{\text{shift}} = \frac{180^\circ + \Delta\varphi}{180^\circ} \cdot \frac{\beta\lambda}{2}. \quad (3)$$

(3) Limitation of total power consumption

As shown in Fig. 1b, a single 500 kW power source is used to provide RF power for both the RFQ and IH-DTL cavity to reduce costs [29]. Considering an RF loss budget of 10% and a standby redundancy of 15%, the total power consumed inside the cavities of the RFQ and DTL must be less than 400 kW with a duty factor of 0.1%. Therefore, the cavity shunt impedance should be carefully optimized for the entire design process. The RF power is partially transmitted to the RFQ and partially transmitted to the IH-DTL by a power divider. The phases are adjusted independently by two phase-shifters to avoid the phase differences caused by the asymmetric transmission path. Additionally, a low-level RF is adopted to control the stability of the amplitude and phase.

(4) Energy difference and phase width of the first gap in the zero-degree section

By adjusting the energy (E_t) and phase advance (φ_t) in the first gap of each zero-phase section, the desired output parameters can be gradually optimized to match the following sections.

(5) Number of bunching and acceleration gaps

The ratio between the number of bunching gaps and acceleration gaps is typically between 1:2 and 1:4, and the number of bunching gaps should range from two to seven per section. In this design, three gaps were adopted in the re-bunching section.

(6) Effective voltage distribution

The effective gap voltage distribution should be considered to reduce the probability of sparking according to the following Kilpatrick empirical equations [30, 31]:

$$f_r [\text{MHz}] = 1.643E_k^2 e^{-8.5/E_k}, \quad (4)$$

$$E_{s,\text{max}} = bE_k, \quad (5)$$

where f_r is the operation frequency (MHz), E_k is the Kilpatrick breakdown field (MV/m), $E_{s,\text{max}}$ is the maximum surface electric field, and b is the reference coefficient for the improvement of technology. The acceptable maximum surface electric field is set to 35.6 MV/m, and the corresponding Kilpatrick coefficient value is 2.0 because the maximum duty factor is 0.1%.

In this design, it is assumed that the voltage at the drift gap varies linearly, which is expressed as

$$V_n = V_2 + (n - 2) \times \Delta V, \quad (6)$$

where V_n is the voltage of the n th gap, excluding the first and last gaps, which are typically set to half the voltage of the adjacent gaps. The voltages of the first, second, and last gaps are set to V_{e1} , V_2 , and V_{e2} , respectively. The voltage growth is $\Delta V1$, and V_{e1} and V_{e2} are used to adjust the output energy.

Based on the former expressions and assumptions, the structure of the KONUS DTL can be described by two structural parameters (i.e., D/L and G/d) and six other parameters (i.e., φ_t , L_t , E_t , V_2 , n , and ΔV). D and G are the lengths of the drift tube and gap, respectively, L is the cell length, and d is the inner diameter of the drift tube.

3.2 Parameter iterative optimization code

After the dynamics principle and preliminary design scheme were determined, optimization code was developed. The main computation process combines the dynamics design and simulation programs (LORASR) based on parameter optimization using the algorithm proposed by Pu [32]. There is a predetermined cost function defining an independently adjustable weight for each design index (i.e., transmission efficiency, output beam energy, maximum axis electric field, minimum drift tube size, and emittance growth) to evaluate design results. A detailed optimization flowchart is presented in Fig. 4. This process is mainly composed of the following two parts.

(1) Initial design

A set of initial parameters is designed, the initial values of the parameters are set, and the preliminary structure of the accelerator is generated to meet certain design requirements.

(2) Optimization process

Optimization is divided into two main parts: optimization of structure and optimization of parameters. Based on the initial design scheme, the structural parameters D/L and G/d are optimized. The best scheme is recorded, and a nonlinear algorithm is applied to change two of the six remaining parameters by a predetermined amount. New structure data are then generated and fed into the LORASR code to perform calculations and simulations. The results are then evaluated and compared. If the new result is better, then the new scheme is recorded and optimization continues. If the new result is worse, then the new scheme is ignored and a new optimization loop begins by changing other parameters based on the former scheme. This process is repeated until the output beam meets the design

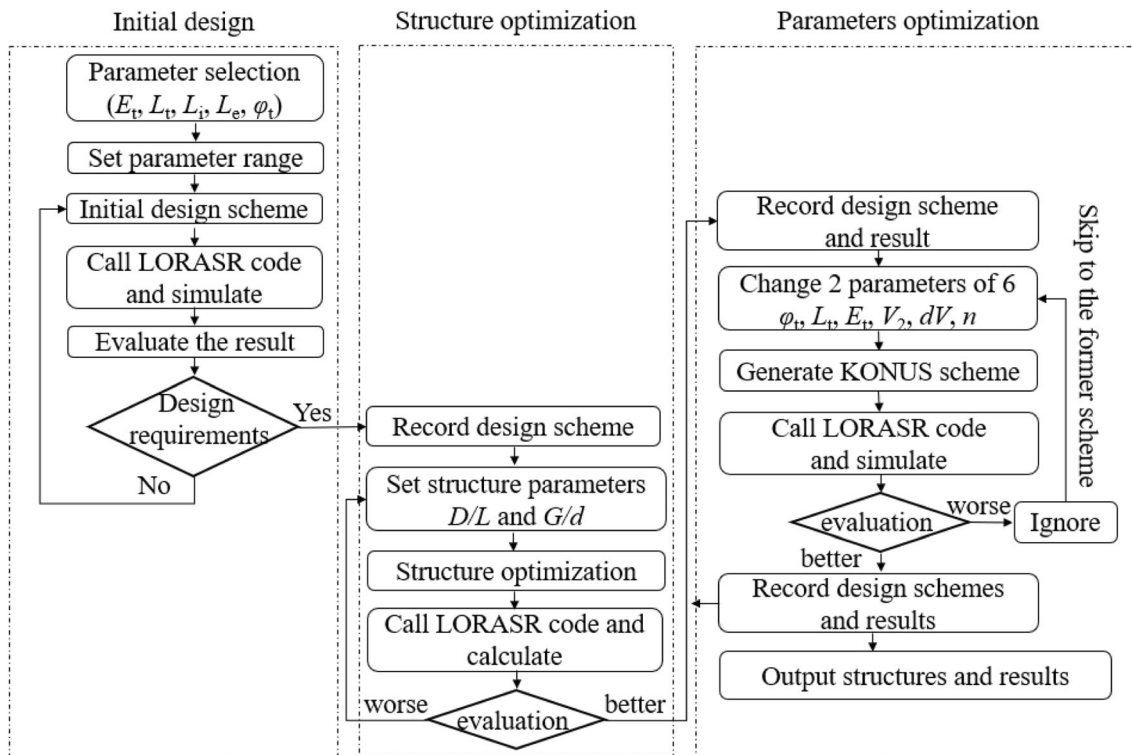


Fig. 4 Flowchart of the optimization process for KONUS DTL dynamics design

requirements. Solutions that meet the design requirements and their corresponding results (listed in Table 1), namely the transmission efficiency, output emittances, emittance growths, output energy, output energy spread, output phase width, minimum drift tube size, maximum axis electric field ($E_{a,max}$), and maximum gap voltage ($V_{g,max}$), are recorded and outputted for reprocessing. Finally, the best scheme is selected by comparing the results of the output schemes and weighing various aspects outside the LORASR code.

3.3 Dynamic results comparison

For the proposed 325 MHz KONUS IH-DTL, the input parameters are listed in Table 4.

Table 4 Input twiss parameters

Input twiss parameters	α	β (mm/mrad)	$\epsilon_{n,rms}$ (π mm mrad)
x	2.84	0.96	0.21
y	2.87	0.97	0.21
Input twiss parameters	α	β (ns/keV)	$\epsilon_{n,rms}$ (keV ns)
z	0	0.0034	2.14

The particles are rapidly accelerated to the target energy of 7 MeV over a total distance of 0.82 m. There are 15 gaps in total with three for longitudinally negative phase bunching (-30°) and 12 for zero-phase acceleration. Figure 5 presents the specific geometric lengths of the drift tubes and gaps, which gradually increase with increasing energy. The transition cell is longer than the adjacent tubes to modulate the synchrotron phase from negative phase to zero phase.

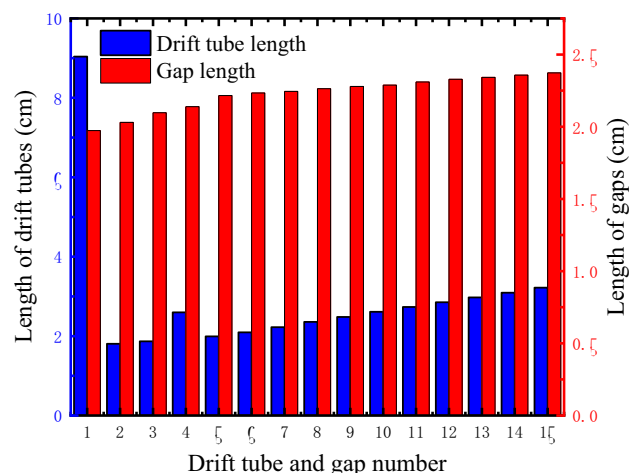


Fig. 5 (Color online) Geometric lengths of the drift tubes and gaps

For the 325 MHz APF, the synchronous phase varies in different gaps within the range of -90° to 90° in accordance with a certain pattern. This is the most crucial aspect of the design process. There are a few phase-variation patterns, such as the symmetric pattern, asymmetric strategy, modified type, stepped-changed phase mode, and Iwata scheme. The Iwata phase variation scheme was adopted in this study. The resulting synchronous phase change is described by the following formula [7, 9]:

$$\varphi_s(n) = \varphi_0 e^{-a \cdot n} \sin\left(\frac{n - n_0}{b \cdot e^{c \cdot n}}\right). \quad (7)$$

Figure 6 presents the synchronous phase arrangement of APF. There are 32 gaps in total. The first several synchronous phases are close to -90° to provide a bunching effect and improve capture efficiency. Additionally, the final few gaps are set at approximately -90° to improve the quality of the extracted beam, while several gaps are close to 90° to provide a focusing effect to ensure stability in the transverse direction. This scheme of bunching and focusing particles by alternating synchrotron phases leads to coupling effects in the transverse and longitudinal directions, resulting in emittance growth in all directions.

The results of the iterative optimization process of the proposed KONUS DTL are listed in Table 5, as well as comparisons to an APF DTL [33, 34]. The cavity lengths are significantly different when using different dynamic principles. The cavity length when using KONUS is half of that when using APF, which is mainly attributed to differences in the synchronous phase. The acceleration gradient is approximately 4.88 MV/m for KONUS, which is approximately twice that of APF. This leads to a direct decrease in cavity length and power consumption for the same output energy and operation frequency. The estimated RF power consumption of KONUS is approximately 180 kW, which is slightly less than that of APF. This value will be further optimized in the following process of electromagnetic design. Additionally, the transit time factors, which gradually increase with different values of β , are approximately 0.85. To meet the cell arrangement and beam requirements, $E_{s,\max}$ should be optimized and simulated as less than 35.6 MV/m, which corresponds to a

Kilpatrick coefficient of 2.0 when the maximum duty factor is less than 0.1% during the design and operation processes. The detailed distribution of the acceleration electric field is presented in the following section.

3.4 Acceleration electric field

Figure 7 presents the phase distribution of the bunch center in each gap of the proposed KONUS IH-DTL. Particles are bunched and accelerated around -30° and 0° , which leads to improvement of the overall acceleration gradient. After the geometry of the units is determined, $E_{s,\max}$ can be optimized by increasing the surface area. Therefore, a typical cell composed of two half drift tubes with one gap between them was established to study the relationships between $E_{s,\max}$, $E_{a,\max}$, and $V_{g,\max}$. When $E_{s,\max}$ is close to 35.6 MV/m, $E_{a,\max}$ and $V_{g,\max}$ are approximately 13.6 MV/m and 0.354 MV, respectively, which are adopted as the limits of $E_{a,\max}$ and V_n , respectively.

The maximum effective voltages of each accelerating gap and the maximum axial electric field are presented in Fig. 8a, which indicates that the maximum effective gap voltage is approximately 0.352 MV and the maximum axial accelerating electric field is 13.45 MV/m, which is 0.76 times the Kilpatrick limit (17.8 MV/m). The fields in the first and last gaps are optimized to approximately half of those in the neighboring gaps. The estimated RF power dissipation is approximately 180 kW. Figure 8b shows the particle energies at every gap center. The proton particles are accelerated steadily from 3.0 to 7.0 MeV.

4 Beam transmission analysis

According to the basic parameters and design principles described above, the basic structure is gradually revealed through iterative operations. The following simulations were performed using LORASR code, and the analytical field was adopted. A total of 6000 macro-particles with a 6D water-bag distribution under different beam currents

Fig. 6 (Color online) Synchronous phase arrangement the 325 MHz APF with the Iwata scheme

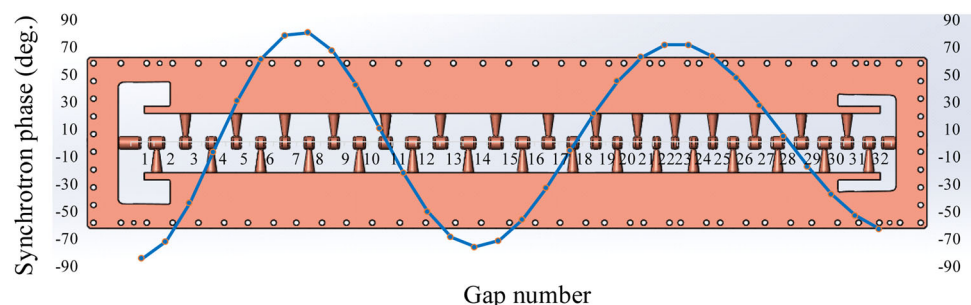


Table 5 Comparison of main parameters between KONUS IH-DTL and APF IH-DTL

Parameters	KONUS design	APF design
Ion type	H ⁺	H ⁺
Frequency (MHz)	325	325
Input/output energy (MeV)	3/7	3/7
Peak current (mA)	18	18
Maximum duty factor (%)	0.1	0.1
Maximum surface electric field (MV/m)	≤ 35.6 ($K_p = 2.0$)	29.5 ($K_p = 1.7$)
Maximum axial field (MV/m)	13.45 ($K_p = 0.76$)	11.57 ($K_p = 0.7$)
Cavity length (cm)	82	152
Power dissipation (kW)	180	195
Tube inner radius (mm)	10	6
Synchronous phase (°)	− 30/0	−90 to 90
Gap number (bunching/acceleration gap)	15 (3/12)	32
Acceleration gradient (MV/m)	4.88	2.64

Fig. 7 (Color online) Bunch center phase arrangement of the 325 MHz KONUS IH-DTL

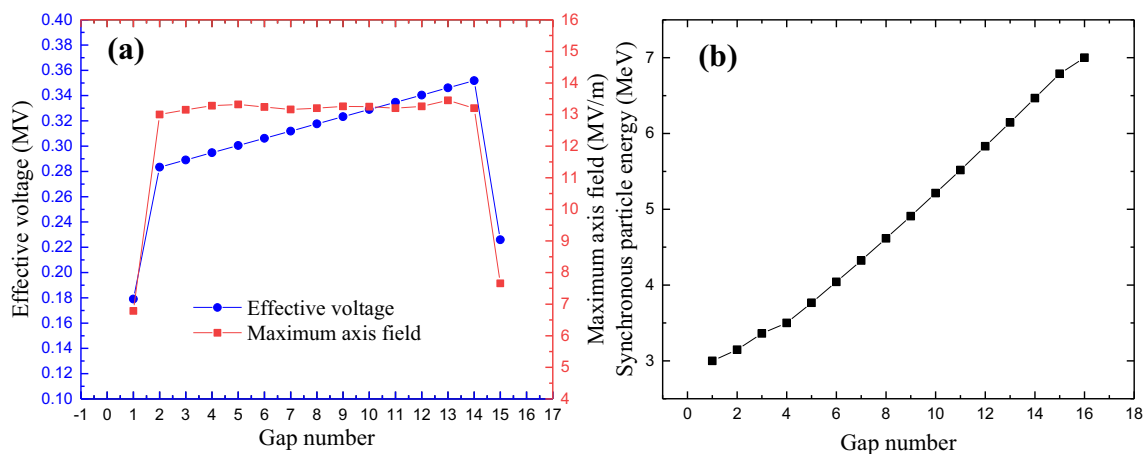
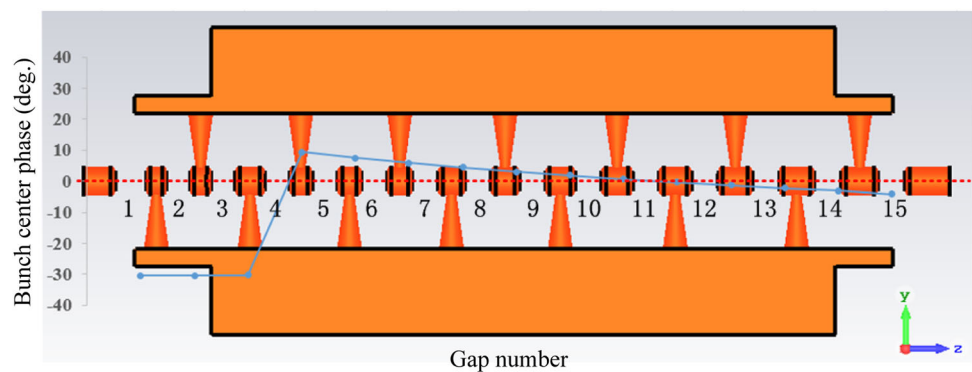


Fig. 8 **a** Effective voltage, maximum axis field, and **b** particle energies at each gap center

were used to evaluate the performance and reliability of the dynamics design.

The longitudinal transmission envelopes along the IH-DTL are presented in Fig. 9a, b under currents of 0 mA, 18 mA, and 24 mA. The solid red lines indicate the energy levels and phases of the bunch centers, whereas the dashed-dotted lines represent the boundaries of the particles. These

boundaries contain 95% of the bunched particles. Both phase envelopes and particle energy levels move asymmetrically downward in the zero-degree section. The phase width and energy spread at 18 mA are greater than those with zero current by approximately 10% and 8.4%, respectively, which can be attributed to the space charge

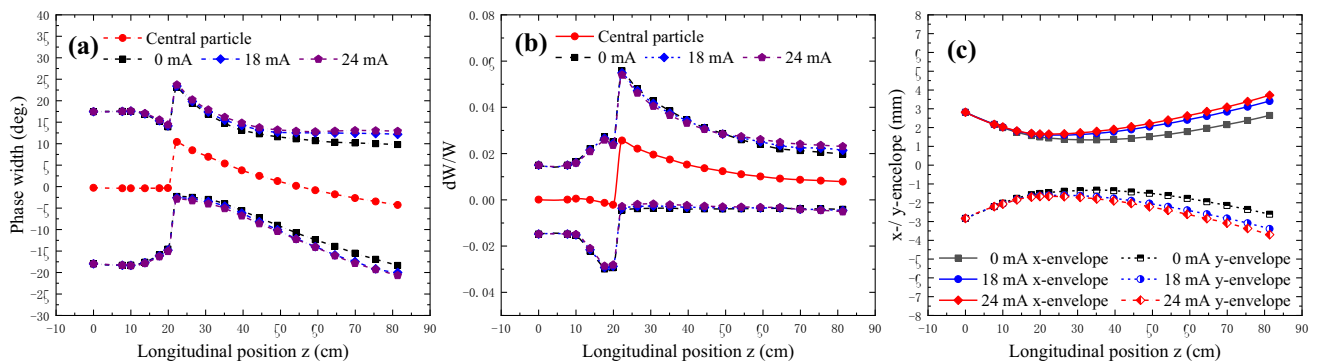


Fig. 9 Longitudinal envelopes (**a** phase width and **b** energy spread) and **c** transverse envelope for 95% of the particles under currents of 0 mA, 18 mA, and 24 mA. Dashed-dotted lines in **a** and **b** indicate the beam centroids (Color figure online)

effect. When the beam current increases to 24 mA, both parameters change by less than 2%.

Figure 9c reveals that 95% of the beam envelopes in the transverse direction are within the range of 1–4 mm for the beam currents of 0 mA, 18 mA, and 24 mA. The beam achieves its maximum radial dimension of 4 mm in the x and y directions at both ends. The inner radius of the drift tubes is 10 mm. The transverse envelopes at full current occupy less than 50% of the area of the aperture, which is sufficiently large to cover all particles and is beneficial in terms of ensuring safe and smooth transmission. With increasing beam current, the transverse radius of the beam also increases, which is mainly attributed to the space charge effect.

The emittance values and corresponding growth rates at the entrance and exit are summarized in Table 6. The growth rates are less than 10% in the horizontal and vertical directions and less than 5% in the longitudinal direction. The distribution and motion of 95% of the bunched particle beam with a current of 18 mA are presented in Fig. 10. At the exit of the zero-degree section, the output energy spread is approximately 1.5% and the output phase width is approximately $\pm 15^\circ$. The beam is extracted and focused by the following quadrupole triplet. The detailed specifications of these lenses will be investigated later to meet the requirements of the synchrotron.

Figure 11a presents the normalized RMS emittance growth along the IH-DTL. The energy dispersion and

phase of the bunch centers at each bunching and acceleration gap are presented in Fig. 11b, which also presents the longitudinal position of the bunched beam centroid for the bunching and acceleration sections. Three bunching gaps with a -30° synchronous phase reduce the phase width of the beam to avoid longitudinal emittance growth. The following section is the 12-zero-synchronous-phases section. At the exit, the particles are accelerated to the target energy and the beam cluster trends toward a defocused state in the transverse direction. A quadrupole triplet is placed at the exit of the cavity to focus the beam in the transverse direction.

Additionally, the tolerance of the input beam current was considered in the LORASR code. Figure 12 presents the beam emittance growth and transmission efficiency as a function of beam current. The target beam current is 18 mA, but an 8–10 mA proton beam that meets the injection requirements of the synchrotron is sufficient for terminal treatment.

Figure 12a presents the beam emittance growth as the beam current changes between 0 and 34 mA. One can see that the emittance grows steadily with an increasing beam current. Until the beam current reaches 24 mA, the longitudinal emittance exhibits exponential growth and the rate of transverse emittance growth increases. Figure 12b presents the transmission efficiency as a function of beam current and reveals that the beam is stable when the beam current is 18 mA. When the beam current increases to 24 mA, the transmission efficiency begins to decrease. Therefore, the operating beam current should be limited to 24 mA to guarantee that the proton beam is in a stable operating state.

Table 6 Normalized RMS emittance values for the input and output beams

Emittance	Input	Output	Growth rate (%)
$x-x'$ (π mm mrad)	0.21	0.23	9.5
$y-y'$ (π mm mrad)	0.21	0.23	9.5
$z-z'$ (keV ns)	2.14	2.2	2.8

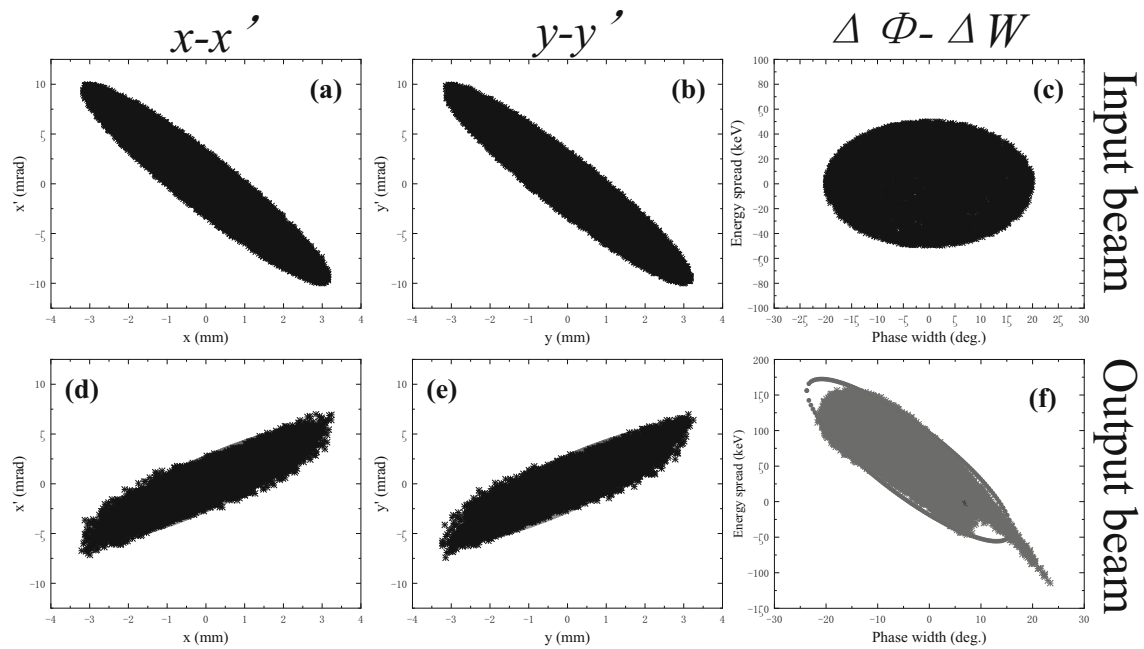


Fig. 10 Particle distributions at a current of 18 mA. **a–c** The input particle distributions in the x , y , and z directions, respectively. **d–f** The output distributions in the same three directions, respectively

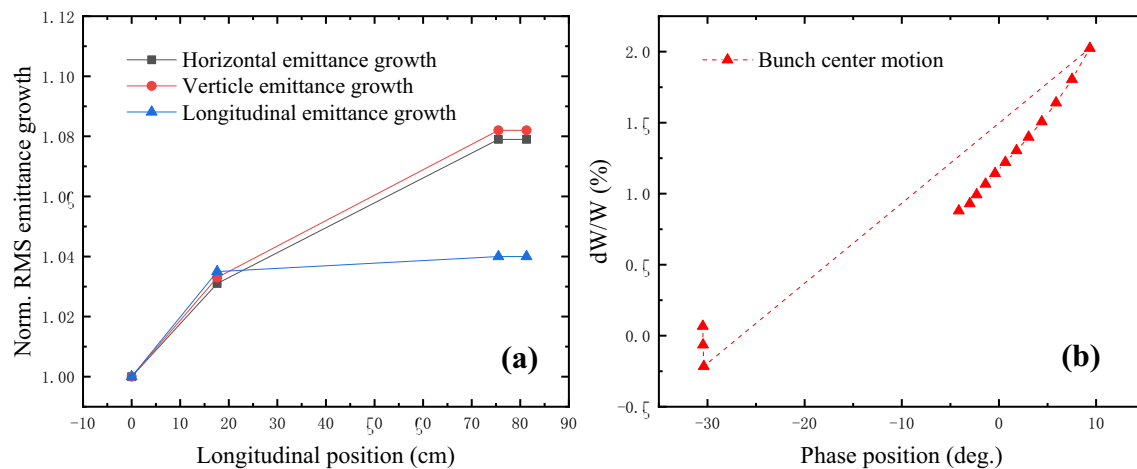


Fig. 11 Multi-particle simulations: **a** Relative normalized RMS emittance growth and **b** longitudinal bunch center motion along the entire cavity

5 Conclusion

In contrast to the NSPS and APF principles, a compact KONUS DTL scheme with no magnet inside the cavity was proposed as a novel domestic linear injector for the synchrotron of the APTR proton therapy complex. Based on the conventional KONUS dynamics principle, a compact proton IH-DTL operating at 325 MHz and a nonlinear optimization method for the injector were developed and simulated using LORASR code. The proton beam was accelerated effectively from 3.0 to 7.0 MeV by a single cavity with a length of 0.82 m. The transmission efficiency reached 100%, and the total energy gain per unit length

was approximately 4.88 MeV/m. Our design strategy, parameter selection process, and simulation results were presented in this paper. It was demonstrated that under the constraint of ensuring 100% transmission efficiency and 18 mA of current, the emittance growth of the optimized IH-DTL is less than 10.0%, which meets the overall design requirements for the proposed linear injector.

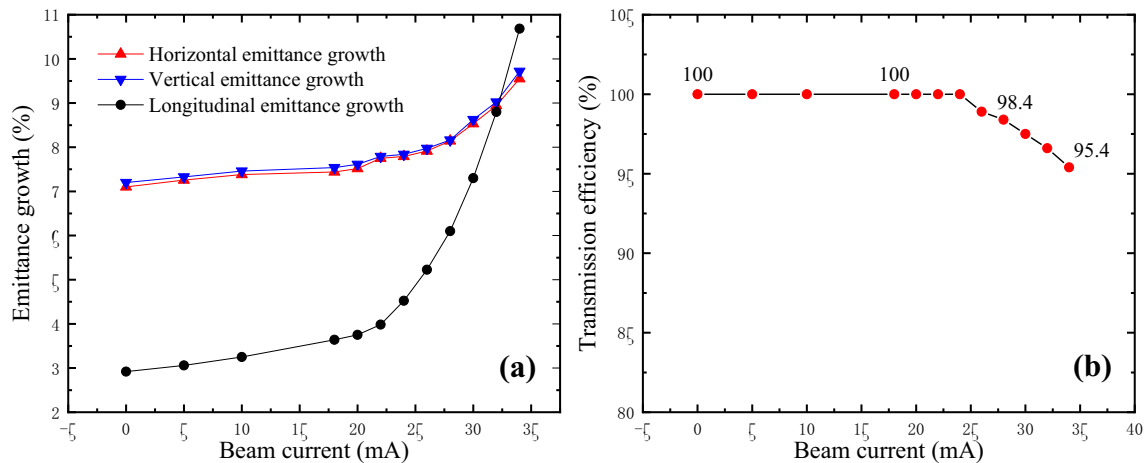


Fig. 12 Robustness analysis: **a** Beam emittance growth versus input beam current and **b** transmission efficiency versus input beam current

References

- O. Jäkel, Radiation therapy with protons and heavy ions. Particle Radiother. (2016). https://doi.org/10.1007/978-81-322-2622-2_9
- T. Chen, X. Li, M. Guo, H. Kong et al., The application of Lynx-2D in proton spot scanning system commissioning. Nucl. Tech. **41**, 050201 (2018). <https://doi.org/10.11889/j.0253-3219.2018.hjs.41.050201>. (in Chinese)
- Y. Ge, C. Yin, Z. Li et al., Optimization design of a multilayer ionization chamber. Nucl. Tech. **42**, 60202 (2019). <https://doi.org/10.11889/j.0253-3219.2019.hjs.42.060202>. (in Chinese)
- G. Han, W. Qin, B. Liu et al., Dynamic magnetic measurements of a Kicker magnet for a proton therapy facility. Nucl. Tech. **43**, 010201 (2020). <https://doi.org/10.11889/j.0253-3219.2020.hjs.43.010201>. (in Chinese)
- S. Fang, X. Guan, J. Tang et al., ATPF—a dedicated proton therapy facility. Chin. Phys. C **34**, 383 (2010). <https://doi.org/10.1088/1674-1137/34/3/015>
- U. Ratzinger, H. Hähnel, R. Tiede et al., Combined zero degree structure beam dynamics and applications. Phys. Rev. Accel. Beams **22**, 114801 (2019). <https://doi.org/10.1103/PhysRevAccelBeams.22.114801>
- Y. Iwata, T. Furukawa, T. Kanai, et al., Beam dynamics of alternating-PHASE-focused linacs for medical accelerators, in *Proceedings of APAC 2004*. [https://doi.org/10.1016/0168-9002\(89\)90289-1](https://doi.org/10.1016/0168-9002(89)90289-1)
- K. Yamamoto, H. Tanaka, H. Harada et al., Experimental verification of an APF linac for a proton therapy facility. Nucl. Instrum. Methods Phys. Res. Sect. B **269**, 2875–2878 (2011). <https://doi.org/10.1016/j.nimb.2011.04.046>
- Y. Iwata, K. Noda, Design of a post linac for an energy upgrade of a heavy-ion injector. Nucl. Instrum. Methods Phys. Res. Sect. B **331**, 10–14 (2014). <https://doi.org/10.1016/j.nimb.2013.09.041>
- U. Ratzinger, R. Tiede, Status of the HIF RF linac study based on H-mode cavities. Nucl. Instrum. Methods Phys. Res. Sect. A Accel. Spectrom. Detect. Assoc. Equip. **415**, 229–235 (1998). [https://doi.org/10.1016/S0168-9002\(98\)00389-1](https://doi.org/10.1016/S0168-9002(98)00389-1)
- T. Murakami, K. Noda, A. Kitagawa, et al., Design and operation of the HIMAC injector, in *Proceeding of Particle Accelerator Conference*. IEEE (1993). <http://doi.org/10.1109/PAC.1993.309098>
- S. Yaramyshev, W. Barth, M. Maier, et al., Upgrade of the HIT injector LINAC-FRONTEND, in *Proceeding of HIAT* (2009). <http://doi.org/10.1109/PAC.1993.309098>
- U. Amaldi, CNAO—the Italian centre for light-ion therapy. Radiother. Oncol. **73**, S191–S201 (2004). [https://doi.org/10.1016/S0167-8140\(04\)80047-1](https://doi.org/10.1016/S0167-8140(04)80047-1)
- Y. Iwata, S. Yamada, T. Murakami et al., Alternating-phase-focused IH-DTL for an injector of heavy-ion medical accelerators. Nucl. Instrum. Methods Phys. Res., Sect. A **569**, 685–696 (2006). <https://doi.org/10.1016/j.nima.2006.09.057>
- M. Maier, W. Barth, W. Bayer, et al., Commissioning of the linac for the heidelberg heavy ion Cancer Therapy Centre (HIT), in *Proceeding of 2007 IEEE Particle Accelerator Conference (PAC)*, Albuquerque (2007). <http://doi.org/10.1109/PAC.2007.4440558>
- H.C. Liu, S.N. Fu, J. Peng, et al., DTL construction status of CSNS project, in *Proceeding of LINAC2014, Geneva, Switzerland* (2014)
- Y. Xiao, Z. Chen, Y. Yang et al., Development progress of the neutron imaging station in CPHS. Phys. Procedia **69**, 96–103 (2015). <https://doi.org/10.1016/j.phpro.2015.07.014>
- H. Eickhoff, R. Bar, A. Dolinskii, et al., HICAT—The German hospital-based light ion cancer therapy project, in *Proceeding of PAC03* (2003). <https://doi.org/10.1109/PAC.2003.1289012>
- White for the SNS Project, M. Marion. Spallation neutron source (SNS), in *Proceeding of AIP Conference Proceedings*, p. 613 (2002). <http://doi.org/10.1063/1.1472000>
- T.P. Wangler, *RF Linear Accelerators*, 2nd edn. (Wiley, New York, 2010). <https://doi.org/10.1002/9783527623426.ch7>
- S. Minaev, U. Ratzinger, B. Schlitt. APF or KONUS drift tube structures for medical synchrotron injectors—a comparison, in *Proceeding of the 1999 IEEE Particle Accelerator Conference* (1999). <http://doi.org/10.1109/PAC.1999.792368>
- M. Bres, A. Chabert, J. C. Gavet, et al., Study on interdigital H-type structure for heavy-ion linear accelerator, in *Proceeding of the 3rd IEEE Particle Accelerator Conference*, vol. 16, pp. 372–376 (1969). <http://doi.org/10.1109/TNS.1969.4325255>
- Y. Lu, Development of an IH-DTL injector for the Heidelberg cancer therapy project. Ges. für Schwerionenforsch. (2005). <https://doi.org/10.1021/jf60214a029>
- U. Ratzinger, *H-Type Linac Structures* (CERN Accelerator School, Lufthansa Training Center, Berlin, 2000)
- R. Tiede, U. Ratzinger, H. Podlech, et al., KONUS beam dynamics designs using H-mode cavities, in *Proceeding of Hadron Beam 2008* (2008)
- R. Tang, Q. Xing, S. Zheng et al., IH-DTL design with modified KONUS beam dynamics for a synchrotron-based proton therapy system. Nucl. Instrum. Methods Phys. Res. Sect. A Accel.

- Spectrom. Detect. Assoc. Equip. **920**, 50–57 (2018). <https://doi.org/10.1016/j.nima.2018.10.125>
27. R. Tiede, G. Clemente, H. Podlech, et al., LORASR Code development, in *Proceedings of EPAC2006, Edinburgh, Scotland* (2006)
28. <https://www.3ds.com/products-services/simulia/products/cst-studio-suite/>
29. P.F. Ma, S.X. Zheng, X.D. Yu et al., Physical design of a single-amplifier-driven proton linac injector for a synchrotron-based proton-therapy system in China. *Nucl. Instrum. Methods Phys. Res. Sect. A Accel. Spectrom. Detect. Assoc. Equip.* **900**, 32–39 (2018). <https://doi.org/10.1016/j.nima.2018.05.047>
30. W.D. Kilpatrick, Criterion for vacuum sparking designed to include both RF and DC. *Rev. Sci. Instrum.* **28**, 824–826 (1957). <https://doi.org/10.1063/1.1715731>
31. A. Liu, X. Wang, J. Liang et al., Design and simulation of vacuum system in energy selection section for HUST-PTF. *Nucl. Tech.* **42**, 12050 (2019). <https://doi.org/10.11889/j.0253-3219.2019.hjs.42.120503>. (in Chinese)
32. Y. Pu, Japan Patent, N. O. 3739575 (2005)
33. X. Xie, Y. Pu, F. Yang et al., Design of a 7-MeV APF DTL with robust considerations. *Nucl. Instrum. Methods Phys. Res. Sect. A Accel. Spectrom. Detect. Assoc. Equip.* **908**, 49–59 (2018). <https://doi.org/10.1016/j.nima.2018.08.028>
34. X. Li, Y. Pu, F. Yang et al., RF design and study of a 325 MHz 7 MeV APF IH-DTL for an injector of a proton medical accelerator. *Nucl. Sci. Tech.* **30**, 135 (2019). <https://doi.org/10.1007/s41365-019-0657-4>